Macromolecules

pubs.acs.org/Macromolecules Article

Solvent Processing and Ionic Liquid-Enabled Long-Range Vertical Ordering in Block Copolymer Films with Enhanced Film Stability

Ali Masud, Wenjie Wu, Maninderjeet Singh, Wafa Tonny, Ali Ammar, Kshitij Sharma, Joseph W. Strzalka, Tanguy Terlier, Jack F. Douglas,* and Alamgir Karim*

Cite This: *Macromolecules* 2021, 54, 8512–8525 Read Online

ACCESS | Metrics & More | Article Recommendations | Supporting Information

ABSTRACT: Rapid and reliable processing methods for forming ordered block copolymer (BCP) materials with low defect density in a thin film geometry are required for many nanotechnology applications. Vertically aligned BCP structures, in particular, have applications ranging from nanolithography for electronics and photonics applications to nanoporous membranes for water remediation and novel batteries for flexible electronics. However, the attainment of a nearly complete vertical orientational order of the BCP-ordered phase remains challenging. Solvent-based techniques, such as direct immersion annealing (DIA) and solvent vapor annealing (SVA), have immense potential for these applications of BCP films, as it allows for a 'tuning' of their thermodynamic, structural, and chain mobility-driven kinetic properties. We first demonstrate that DIA, using a judicious choice of binary solvent mixtures, along with a relatively hydrophobic ionic liquid (IL), induces the rapid vertical ordering in polystyrene-*b*-poly(methyl methacrylate) (PS-PMMA) in lamellae-forming block copolymer films. The IL in a binary solvent mixture with toluene and heptane apparently gives rise to a near-neutral solvent for the BCP for itself and the boundary that is useful for attaining the vertical microstructure within the BCP film. Next, we show that an IL can moreover suppress the dewetting of the PS-PMMA films to achieve long-range order using SVA in cylindrical films after long annealing times. Both vertical and horizontal morphologies are attained in these films by selecting different solvent conditions. Attaining enhanced vertical and horizontal BCP structures with long-range defect-free order by tuning solvent quality and using additives like ILs can render them useful for many nanotech applications.

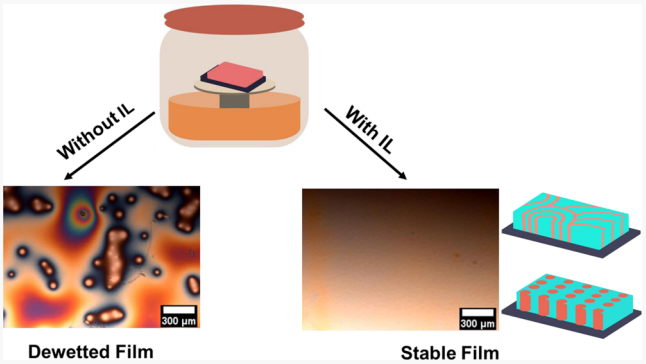

INTRODUCTION

The directed self-assembly (DSA) of block copolymers (BCPs) to form periodic, repetitive structures on the scale of 5−50 nm[1] has been perceived as a cost-effective alternative to photolithography and potentially has a myriad of applications in nanoelectronics,[2] optoelectronics,[3,4] energy storage,[5−7] and other forms. A higher Flory−Huggins interaction parameter χ in BCPs enhances their tendency to phase separate due to a higher thermodynamic driving force.[8] However, many BCPs, such as polystyrene-*b*-poly(methyl methacrylate) (PS-PMMA), have a relatively small positive χ (≈0.04), and the kinetics can be slow due to a high T_g, which can lead to higher line edge roughness, lower period alignment, and a higher defect density.[1,9,10] A low χ nevertheless is a significant advantage in lithographic pattern translation due to the easy removal of one block using wet etching or plasma etching,[11] BCP with low χ_i values have been widely used in growing industrial applications of these materials. As such, DSA of the BCPs based on novel processing techniques is a promising approach for improving the long-range pattern formation, with reduced defect density and faster kinetics.[12]

There is then a need for a solvent-based processing technique that can alter the thermodynamic interaction between the blocks[9] and also provide a medium through the liquid surface to interact with the polymer to form more desired vertical features, while providing a higher mobility for enhanced ordering kinetics compared to melt annealing.[13]

Solvent annealing includes two major types, solvent vapor annealing (SVA) and direct immersion annealing (DIA).[9,14,15] SVA is a well-studied time-intensive processing technique that sets up an equilibration of the vapor pressure of a solvent or a mixture of different solvents, and the relative affinity to each block determines how the solvent partitions in the polymer blocks and affects the overall BCP χ. Subsequently, the solvent−polymer interaction determines the thermodynamic and

Received: June 17, 2021
Published: September 17, 2021

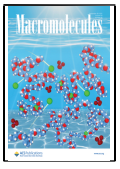

https://doi.org/10.1021/acs.macromol.1c01305
Macromolecules 2021, 54, 8512−8525

diffusive motion of the polymer blocks, inducing order.[16] SVA is an established and useful annealing technique having the advantage of reducing defect density, enhancing the grain size of the repetitive structure, and controlling domain morphology and size.[16−18] Solvent vapor annealing has been extensively used for high χ BCPs with low mobility of polymer chains and may take up to a few dozens of hours to order.[19] The diffusive motion of polymer segments perpendicular to the domain interface during the ordering process is expressed as $D \sim D_o \exp(-\alpha\chi N_A)$, where D_o is the kinetic perfector that is a strong function of $T-T_g$, and N_A is the degree of polymerization of the block that is drawn into the unfavorable domain.[20]

DIA, on the other hand, is a relatively new polymer film processing technique demonstrated by Park et al. to order high χ BCPs to form ultrafast ordered BCPs in the sub-20 nm regime with high pattern fidelity.[21] Modi et al. further developed DIA to order and orient a cylinder-forming low χ PS-PMMA to obtain long-range order with enhanced kinetics while establishing that the activation energy for the process was much lower than thermal annealing.[22] Subsequently, Longanecker et al. used DIA with selective solvents to demonstrate ultrafast kinetics of BCP film ordering with nanofillers, a material that is typically particularly sluggish to process by thermal annealing. This work also indicated an unexpected reduced domain size by as much as 50%, along with interfacial sharpening in lamellae forming low χ PS-PMMA materials where these enhanced properties were quantified through an extensive neutron reflectivity (NR) study.[9] In DIA, the immersion of the film inside a carefully designed miscible solvent mixture allows for a controlled, yet rapid, film swelling, enhanced chain mobility, and altered thermodynamic properties to attain the desired feature(s) in a relatively short time. Both DIA and SVA require a meticulous control of the solvent mixture by solvent type and composition since selective and neutral solvent typically used in these systems may cause significant swelling or have too high a solubility overall for the BCP and readily lead to film dissolution or dewetting if the solvent mixture has properties that disrupt the wetting of BCP to the substrate. As such, a large fraction of a poor solvent for both BCP components must be present to suppress these adverse effects. The judicious choice of solvent components and at appropriate fractions clearly offers the potential to tune the morphological structure, periodicity of the repetitive structure, and kinetics of ordering.

Recently, ionic liquids (ILs), essentially a type of organic salt, have found applications in several areas in polymer science, such as in the synthesis of polymer electrolytes for batteries, membranes, fuel cells, etc.[23] ILs have the advantage of being molten at room temperature, with negligible vapor pressure, are nonflammable, and have excellent thermal stability, higher operating temperature range, and improved safety.[23] ILs can selectively associate with a particular polymer by physical forces such as the van der Waals (VDW), and its lower cohesive energy density helps it to enhance the segregation coefficient in BCP systems and alters the surface energy. In BCPs, such as PS-PMMA, certain ILs were found to associate with the PMMA block of the copolymer and enhance the mobility of the block like a plasticizer, reducing the glass-transition temperature of the BCP.[24] Interestingly, they have also been shown to increase the Flory−Huggins interaction parameter, χ, in BCPs, thereby enabling ordering in low N BCP systems with smaller feature size.[24,25]

Apparently, the first use of an IL to process a BCP materials was Bennett et al., where it was shown that adding a small amount of IL such as 1-ethyl-3-methylimidazolium bis-(trifluoromethane sulfonyl)amide (EMIM NTf_2) can enhance χ parameter, studied from the domain swelling of the PS-PMMA revealed by small-angle X-ray scattering (SAXS) ($L_o \sim \chi^{1/6}$), and enable order in a low N system that would not otherwise order.[24,25] Moreover, they also found that ILs can induce morphological transition in hexagonally ordered cylindrical films to lamellar morphology when used in excess due to domain swelling of the minority cylinder-forming block. More recently, Chen et al. have demonstrated a similar effects in a low M_w BCP material to attain nanopattern pitches below 20 nm.[26] Earlier, Ye et al. studied the use of an IL with PS-PMMA to order cylindrical systems using rotational cold zone annealing, a combinatorial method to optimize the velocity and time in zone annealing in melt state[3] to attain perpendicular cylinder orientation due to change in surface tension and segmental relaxation.[27,28] Quite recently, we have shown that adding IL to symmetric PS-PMMA lamellar system can help induce substrate-driven lamellar stratification in thicker and high M_w systems that otherwise would be arrested in a metastable defect state or not order at all when ordered using thermal annealing. Such enhancement in the extent of ordering of the BCP was atrributed to the enhanced molecular mobility and increase in the thermodynamic segregation parameter χ found using neutron reflectivity. Moreover, it was also shown that annealing the films at an elevated temperature in vacuum conditions removes about 99% of the IL.[29]

In this paper, we demonstrate the ability of both the solvent processing techniques of DIA and SVA to enhance the vertical ordering in lamellar and cylindrical films facilitated by the presence of ILs in the cast films. The presence of IL in the films and solvent processing methods also helps us to improve the long-range and defect-free order, arising from an increase in χ between the PS and IL-solvated PMMA blocks while balancing the segmental interactions with the silicon substrate to suppress dewetting in these films in the solvent-swollen environment. Importantly, PS-PMMA BCP films cast from a good solvent such as toluene with a small percent of added IL, combined with solvent processing methods with a neutral solvent design, are shown to drive the perpendicular orientation of PS-PMMA domains in these systems validated in the medium M_w PS-PMMA (33k−33k) and low M_w (10k−10k) lamellar systems. The IL thermodynamic enrichment of χ appears self-saturating, as confirmed by the little change in domain structure with an increased amount of IL beyond a limiting value when processed through DIA, with vertical morphology validated through grazing-incidence small-angle X-ray scattering (GISAXS) and UV etching of the films. The enhancement in the thermodynamic parameter was quantified using neutron reflectivity measurements and showed an almost doubling of the χ. The SVA-annealed films retain the IL by design and have a higher enhancement in orientational order, as confirmed by atomic force microscopy (AFM) and GISAXS. These findings provide a useful framework for designing vertically oriented BCP films using a roll-to-roll compatible DIA and SVA method for applications such as in nanolithography, membrane design, energy storage, etc.

MATERIALS AND METHODS

Film Preparation. Block-co-polymer of PS-PMMA of M_n = 66k (33k−33k, L-BCP), PDI = 1.09, 20k (10k−10k, L-BCP), PDI = 1.05 lamellar morphology, and M_n = 77k (55k−22k, C-BCP), PDI = 1.09 cylindrical morphology, were purchased from Polymer Source Inc. The

https://doi.org/10.1021/acs.macromol.1c01305
Macromolecules 2021, 54, 8512−8525

as-received polymers were measured using microbalance to make a solution of 4−8 wt % of polymer solution in toluene as solvent. IL, 1-ethyl-3-methylimidazolium bis(trifluoromethylsulfonyl) imide ([EMIM][TFSI]),[30] purchased from TCI Chemicals, was dissolved in tetrahydrofuran (THF) and mixed to the polymer at an appropriate weight fraction. A 2−4 wt % polymer/IL solution was obtained, diluting the mixture using toluene. Films were cast using a flow coating machine at speed (1−2) cm s^{-1} to get a film of thickness of about 60−150 nm. The thickness of the as-cast films was measured using the Film metrics LSDT2 system after drying for 24 h at 50 °C in a vacuum oven to remove the residual solvent.

Direct Immersion Annealing (DIA)/Solvent Vapor Annealing (SVA). DIA or SVA was performed in a toluene and heptane solvent mixture (mixed in a ratio of 1:3 by relative volume fraction) or pure toluene or acetone solvent vapor using solvent or solvent mixture in a closed chamber at room temperature and pressure. Annealing was performed for 30 min (DIA) to 24 h (SVA) and carefully removed from the solvent without altering the film surface. The substrate was held at an angle to rapidly evaporate any residual solvent at room temperature and heated promptly for 15 min at 60 °C to remove residual solvents.

Characterization. The topography of the as-cast and annealed samples was imaged using AFM in the tapping mode. The Bruker AXS Dimension Icon was used in these measurements, which is a state-of-the-art instrument. GISAXS was performed at the Advanced Photon Source of the Argonne National Lab on beamline 8-ID-E40. X-ray with a photon energy of 7.35 keV and a wavelength of λ = 1.6868 Å impinged on the sample at a grazing angle of 0.1−0.2. It is known that the critical angle of the film is 0.11, and the silicon wafer is 0.16. The best intensity for through-thickness penetration was found at an incident angle of 0.14, and it probes the bulk of the film. The reflected waves were detected on a Dectris Pilatus 1 M pixel-array detector. An Argonne-developed software called GIXSGUI was used to convert the data to q space and draw line spaces to get I vs q curves.[31] Optical microscopy images were taken from the Olympus BX41 instrument at 10× magnification. Ultraviolet−ozone (UVO) ablation was performed using a 193 nm UV wavelength device that removes films at a rate of roughly 2.5−3 nm per minute.

A time-of-flight secondary ion mass spectroscopy (ToF-SIMS NCS) instrument was used to attain the positive high-mass-resolution depth profile, which has a ToF, SIMS5 instrument (from ION-ToF GmbH, Münster, Germany) with a scanning probe microscope installed in situ (from NanoScan, Switzerland). The primary probe used for the analysis had bunched Bi^{3+} ions (directed at 30 keV with a measured current of 0.02 pA) and scanned an area of 100 × 100 μm^2. An $Ar1500^+$ ion at 10 keV was used to sputter over a rastered area of 500 × 500 μm^2 with a current typically of 0.3 nA. Non-interlaced mode operation was used for the beams having two cycles per operation, with first the alternating analysis cycle and the second the sputtering cycle (the equivalent of 1.63 s). An electron gun was used for charge compensation with a pause of 3 s between the sequences. A surface potential of −8 V and an extraction bias of 0 V were used for the adjustment of the charge effects during the operation. Depth profiling used a fixed cycle time of 200 μs, which corresponds to a mass range of m/z equivalent to 0−3644 amu.

Neutron reflectivity (NR) data were collected at the NG7 reflectometer instrument at the NIST Center for Neutron Research. A collimated neutron beam at a constant source with a wavelength of 4.76 Å and a divergence of 0.18 Å was used as the emitter. From the wavelength λ and the angle of incidence θ with a range of 0.006−0.16 $Å^{-1}$, the magnitude of the wavevector was derived using the equation $Q_z = 4\pi \sin(\theta)/\lambda$, and the data were subsequently reduced and analyzed using the ReflRed and Reflpak software packages developed at NIST.[32]

RESULTS AND DISCUSSION

The vertical orientation of ordered lamellae forming PS-PMMA on bare silicon in the melt state is a nontrivial task due to the strong preferential attraction of the PMMA block to the silicon oxide surface. In contrast, the free air surface is slightly PS-selective. The surface energy of the UV-treated silicon surface is Υ_{SiO2} = 75.7 mJ m^{-2},[33] whereas Υ_{PS} = 40−42 mJ m^{-2} and Υ_{PMMA} = 41.1 mJ m^{-2}.[33,34] Although the surface energies of the blocks are not very different, the contributing force for the segregation of PMMA to the substrate may be attributed to the individual polar and dispersive components ($\Upsilon_{PMMA,polar}$ = 11.5 mJ m^{-2} vs $\Upsilon_{PS,polar}$ = 6.1 mJ m^{-2}, $\Upsilon_{PMMA,dispersive}$ = 29.6 mJ m^{-2} vs $\Upsilon_{PS,dispersive}$ = 34.5 mJ m^{-2}).[35] The higher polar component of PMMA due to the carbonyl, −C═O, group makes it more attractive to the SiO_2 surface and PS to the free air surface. BCP morphology defined by the intrinsic block composition may be modified by a variety of parameters that include substrate surface energy, roughness, film thickness, molecular weight, annealing temperature, external fields, and incorporated additives. The lamellae in PS-PMMA thin films ($h < 6\ L_0$) are generally oriented parallel to air and a silicon (oxide) substrate interface.[36−39] Thicker films exhibit a more meandering state of the lamellae in the film interior, while maintaining a parallel lamellar structure near the interfaces.[37]

Similarly, cylinder-forming PS-PMMA thick films on bare silicon surface take on a parallel hexagonal cylindrical structure at the substrate surface, transitioning to meandering structures within the film, and can often be parallel or perpendicular at the free surface.[36] However, these results are obscured in high-molecular-mass block copolymer films or at lower annealing temperatures leading to partial short-range order and poorly ordered meandering structures. Depending on the thickness and annealing conditions, nonequilibrium annealing-based processing methods can drive a complete perpendicular cylinder orientation to the silicon substrate, by locking in structures in a metastable state, before surface segregation or wetting of one block component can occur.[35,40,41]

There have been several other methods explored in the literature to obtain vertical structures in lamellae and cylinder-forming PS-PMMA thin films. One of the distinct ways to achieve a near complete perpendicular orientation of the BCP structure is the interfacial engineering of the top and the bottom surfaces to be neutral to both the blocks of the BCP. PS-*r*-PMMA having a 56−60% of PS in the backbone distribution is frequently used to create a neutral surface on a silicon substrate.[42−44] Perpendicular ordering has also been obtained using graphoepitaxy,[1] chemoepitaxy,[26,34] or a combination of both, with side-wall engineering. Other methods such as topcoats with neutral coating on both the interfaces, use of homopolymers with block copolymers,[45] organic additives, and inorganic additives[46] including NPs such as Au NPs,[47] multiple-armed star polymers and processing techniques such as zone annealing,[48] laser annealing, and electric field methods[49] have also been tried. However, most of these methods apply only to ultrathin films, are relatively complicated, time-intensive, expensive, and introduce many process variabilities that are difficult to control.[50]

A simple way to control the microenvironment of the top and the bottom layers is by using a solvent mixture that is neutral to the blocks and renders a neutral environment to blocks and interfaces. A carefully designed solvent and additive mixture can achieve a neutral/near-neutral environment that results in balancing of surface/interfacial tension, γ, to have a neutral impact on both the blocks. Such solvent system strategies have been used by several authors to attain a vertical structure, e.g., SVA of block copolymers like PS-PEO[51] and PS-PDMS resulted in a complete perpendicular ordering using such solvent vapor environment.[52] However, it is desired to attain a perpendicular oriented lamellar/cylindrical structure of PS-PMMA films on the silicon surface due to its optical patternability and etchability

https://doi.org/10.1021/acs.macromol.1c01305
Macromolecules 2021, 54, 8512−8525

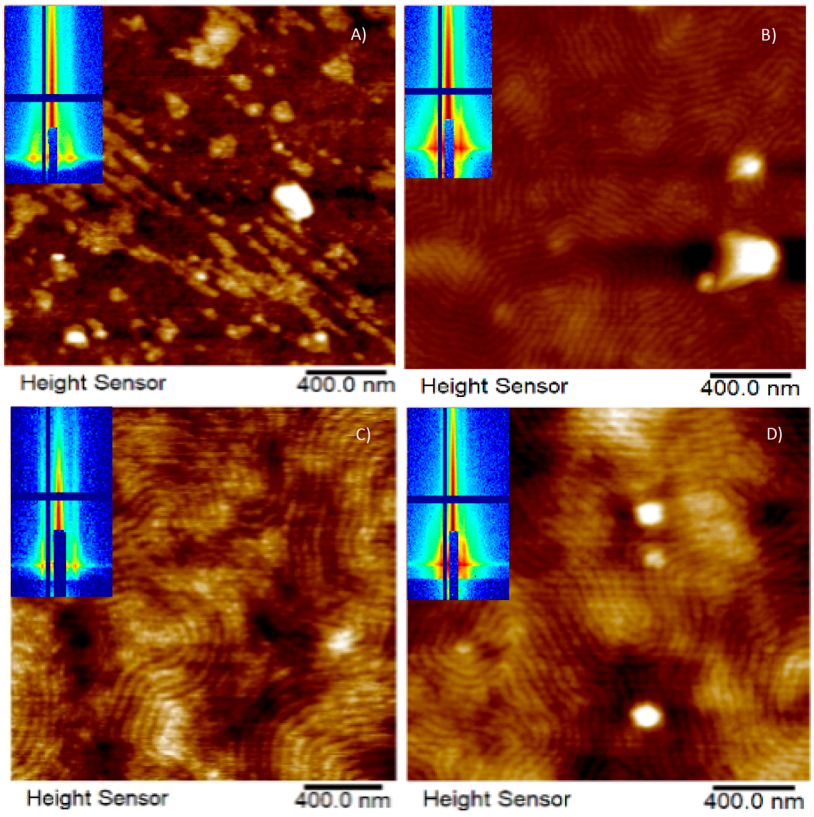

Figure 1. AFM image of the evolution of as-cast films as the percentage of ionic liquid increases from (A) no IL, (B) 4 mass % IL, (C) 8 mass % IL, and (D) 12 mass % IL in films of PS-b-PMMA 33k−33k of a thickness of about 60−70 nm. The inset shows the GISAXS in in-plane (q_x) and out-of-plane (q_z) directions. A small level of the weak homogeneous peak is present at no IL. As the percentage of IL increases, the in-plane peak becomes more potent with the presence of no homogeneity, signifying complete perpendicular orientation in an as-cast film with IL.

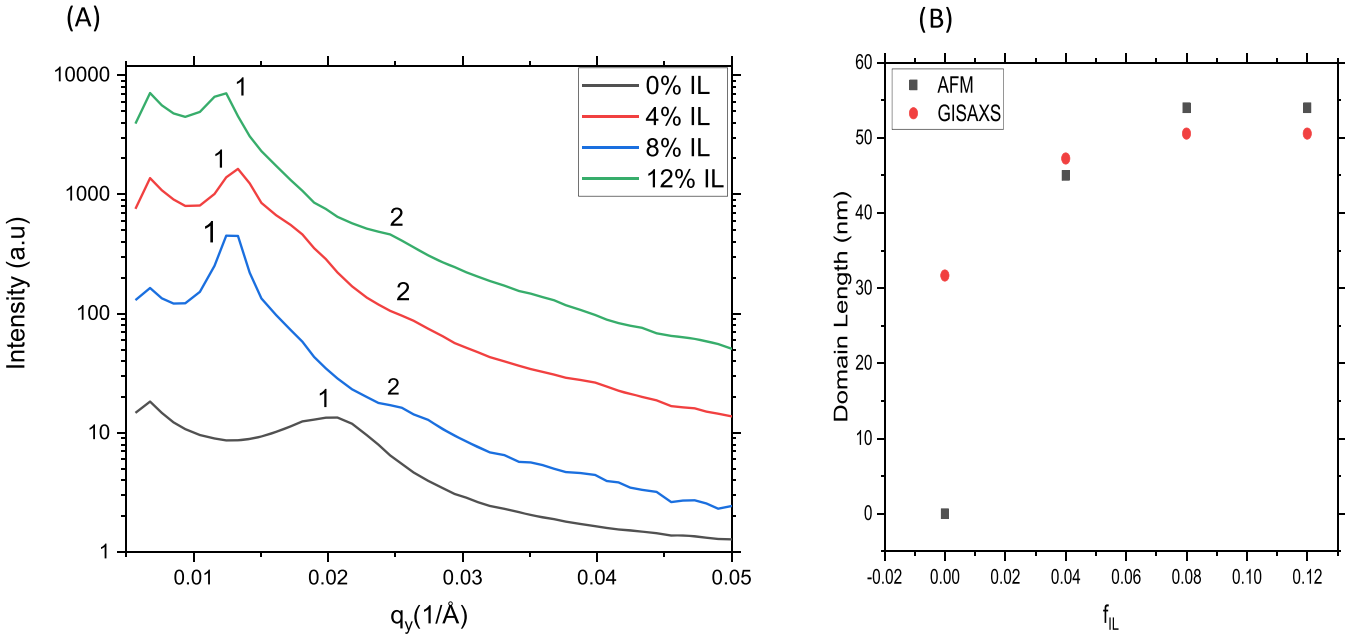

Figure 2. (A) Line-cut from the GISAXS profile shows the in-plane Q_y structure in as-cast l-BCP films. The addition of IL has significantly improved the perpendicular ordering with higher-order peaks, as can be seen here. (B) Domain length using AFM and GISAXS.

with high fidelity. However, PS-PMMA suffers from a low interaction parameter, χ, and in a system of good solvents, it can easily dewet due to enhanced mobility perpendicular to the interface, $D \sim D_o \exp(-\alpha\chi N_A)$,[53] or in a controlled solvent environment, it can attain highly parallel structures without passing through a metastable perpendicular state.[29] We demonstrate in this work that careful choice of additives can help achieve the vertical structure of PS-PMMA without dewetting the film.

https://doi.org/10.1021/acs.macromol.1c01305
Macromolecules 2021, 54, 8512−8525

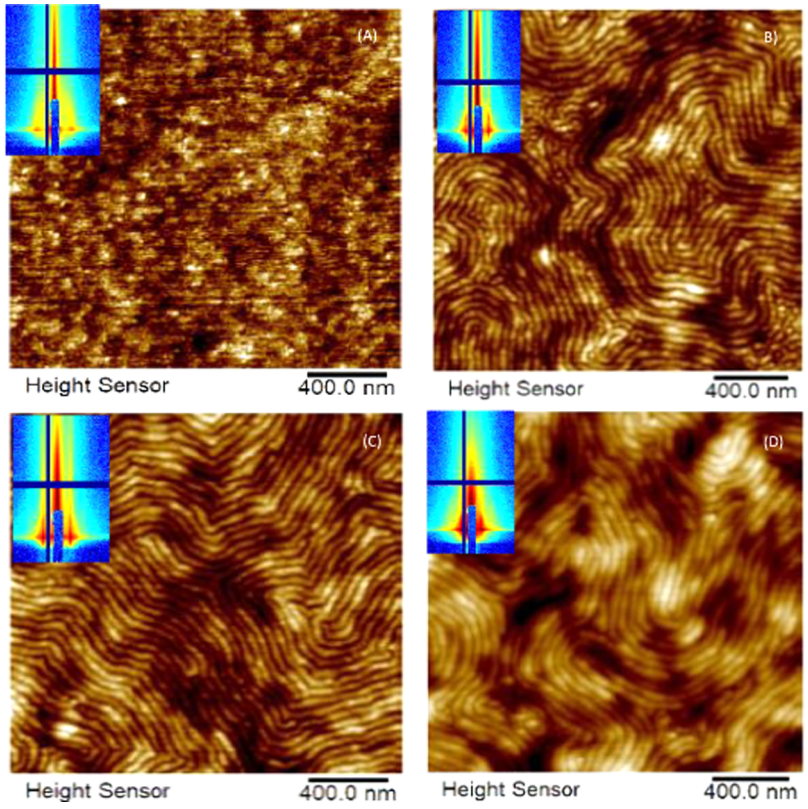

Figure 3. AFM image of films after DIA in a 3:1 heptane to toluene solvent for 30 min without and with IL as the percentage of IL increases from (A) no IL, (B) 4 mass % IL, (C) 8 mass % IL to (D) 12 mass % IL in films of PS-*b*-PMMA 33k−33k of the thickness of about 60−70 nm. The inset shows the GISAXS in-plane (Q_y) and out-of-plane (Q_z). With no IL, vertical ordering is present but is of short range. As the percentage of IL increases (4−8 mass %), the range becomes more extended and the in-plane peak becomes more robust and even more than as-cast films; the absence of any homogeneity signifies complete perpendicular orientation.

We then selected a near-neutral solvent mixture and an additive IL, EMIM TFSI, to control the microenvironment and attain a vertical structure in the lamellar PS-PMMA film ordering morphology that was cast from a toluene solvent-containing IL. The near-neutral solvent mixture, in this case, is a 3:1 relative volume fraction ratio of heptane and toluene mixture. Heptane is a poor solvent and swells PS-PMMA to a low degree, and toluene is a good solvent for both, displaying almost a neutral behavior.[13]

Figure 1 shows the AFM morphology of the films cast by flow coating of PS-PMMA 33k−33k (lamellar, l-BCP) of thickness about 60−70 nm (1−2 L_o). It is seen that without IL, there is no ordering present on the surface. The inset (Figure 1A) GISAXS profile, probing the full film thickness, however, shows the presence of both mixed parallel and perpendicular morphologies. The signal, however, is not very strong, suggesting a lower statistical significance of the ordering present in this system. With the addition of IL to the as-cast films, a perpendicular lamellar structure evolves, as confirmed by the AFM and GISAXS (Figures 1 and 2). The in-plane GISAXS peaks (q_y) get more prominent and oriented (Figure 1B,C) with the addition of 4 mass % IL and 8 mass % IL, signifying a higher degree of perpendicular orientation. The in-plane peaks are sharp but still not as strong as after DIA annealing (as will be seen later in Figure 3). It should be noted, however, that some "clusters" exist in the AFM images, as seen in Figure 1A−C, which appear to be on top of the as-cast films, wherein the BCP seems to have agglomerated and is not ordered properly. This is likely due to the fact that, in as-cast films, the solvent evaporates very fast and the polymer has very less time to reassemble into an ordered phase structure while casting. Nevertheless, the presence of IL has a clearly enhancing effect on the vertical order of morphology in the process.

Figure 2 represents the GISAXS line-cut profile of q_y integrated along all q_z as the amount of IL in the BCP film increases. In Figure 2, the neat as-cast films without IL show the presence of a weak in-plane structure, and the peak is broad and diffused, signifying relatively poor order organized BCP structures, typical of as-cast BCP films. It is also apparent in Figure 2A that in the as-cast film, there is no second-order peak present. It is known that the presence of higher-order peaks is an indication of a high degree of BCP ordering. The first-order peak without IL occurs at q_y = 0.021 and using the Bragg definition $L_o = \frac{2\pi}{q}$, a domain length of 30.2 nm is obtained. We note that using the strong segregation limit, the theoretical domain length would be 37 nm in melt equilibrium films. The lower value signifies domain scale shrinkage, typical in rapidly evaporating solvent-cast L-BCP films.[9] Next, we focus on as-cast L-BCP films with added IL. Interestingly, the addition of IL results in a well-ordered as-cast L-BCP film on a bare Si surface. The IL appears to act as a plasticizer and enables the ordering of the film without thermal or DIA annealing. Notably, the domain length increased in IL-added films to about 50 nm compared to the theoretical domain length of 37 nm due to the swelling of the PMMA block primarily by the IL.

Figure 2 shows that sharp first-order peaks exist in L-BCP films containing IL, with the existence of weak second-order

https://doi.org/10.1021/acs.macromol.1c01305
Macromolecules 2021, 54, 8512−8525

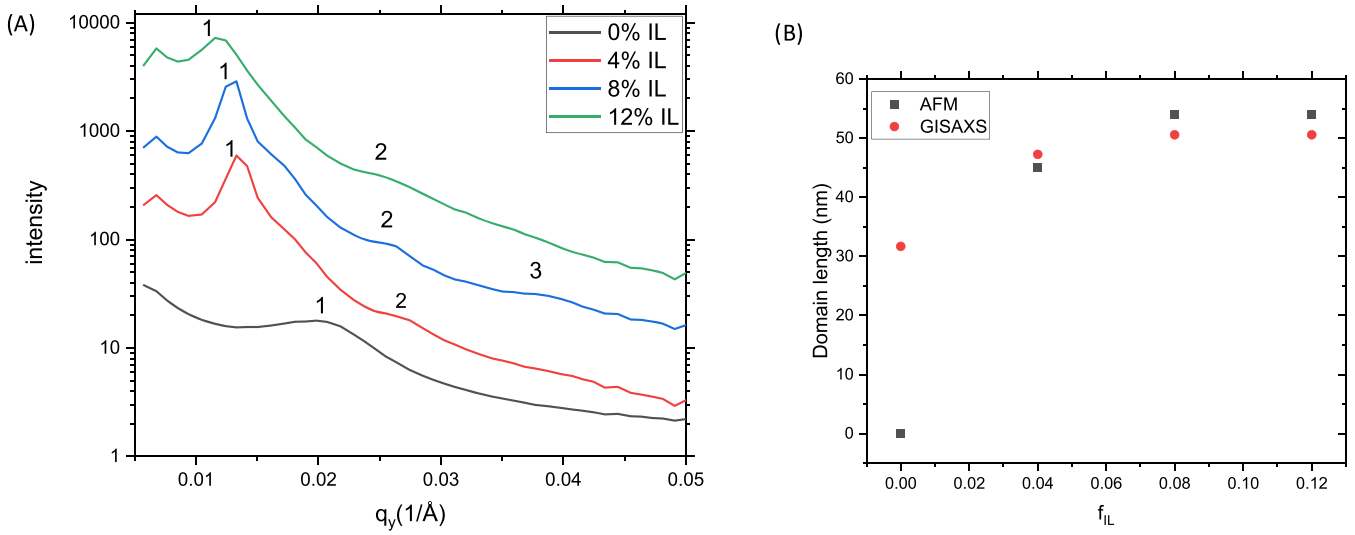

Figure 4. (A) Line-cut from the GISAXS profile to show the in-plane q_y structure after DIA. Although the AFM image without IL shows no in-plane ordering in the surface, GISAXS of the entire bulk structure shows the presence of a weak in-plane structure that is significantly contracted compared to the ordered structure in the presence of IL. Fast evaporation of the solvent to lock films in a metastable structure is known to reduce the domain structure. (B) Domain length obtained from AFM and GISAXS.

peaks. A noticeable hump can be seen in IL-containing films, which can arise due to some asymmetry brought to the lamellar system by the IL due to swelling of the PMMA block, although no morphological transition to substrate parallel hcp-cylinders is observed, as no $\sqrt{3}$ peak is observed. The domain spacings are plotted in Figure 2B. It is apparent from Figure 2B that the domain length increases from 30.3 to 47.2 nm in films containing 4 mass % IL relative to BCP, leveling out to 50.6 nm at higher IL concentrations. The domain length measured from the AFM surface structure closely matches with the domain size from the GISAXS, signifying that the statistical average of the domain length throughout the bulk of the film closely corresponds to the surface features. We note that it would be erroneous to assume that the increase in domain length is purely due to the enhancement of χ (if we assume $L_o \sim \chi^{1/6}$, χ increases from 0.042 to 0.26, which is almost a 6-fold increase), as there is an additional solvent swelling of domain size in the presence of IL acting as a selective solvent for PMMA. Although our findings show that the swelling effect is not highly block-specific, i.e., the entire BCP swells retaining the neat BCP symmetric/asymmetric structure as the IL concentration in the system increases, which could suggest that although IL wets the PMMA block preferentially, but the thermodynamic effect affects the entire BCP with increasing IL content. In general, the IL enhances the Flory–Huggins interaction parameter χ, lowers the glass-transition temperature (T_g) of the polymer mixture, as well as lowers the surface tension of the polymer system.[24] Lowering T_g means that ordering can be induced in the system at a faster pace due to higher mobility of the polymer and segments.

We first used neutron reflectivity to better gauge the influence of IL and DIA processing using parallel-ordered lamellar films. To attain parallel order, we have used a small amount of acetone to the neutral DIA mixture, as acetone is PMMA-selective. We see the formation of long-range defect-free lamellar ordering with 5 mass % IL-containing films after DIA with a reduction of the interfacial width by up to 34.4% and a domain length by 50%. These figures are similar to DIA processing results reported earlier by Longanecker et al., with a higher reduction in the interfacial width of 34.4% as opposed to 27% (see Figure S3).[9]

The synergistic effects of the IL and the solvent processing (DIA) are responsible for such enhancements. As such, the Flory–Huggins interaction parameter, χ, between the blocks increases from 0.041 to 0.073 (an increase of nearly 2 times) using the Helfand interface width ($w \sim \frac{1}{\sqrt{\chi}}$) approximation in the SSL limit.[54] The effects of the IL on χ are profound in the (0–4) mass % IL; however, this is best calculated from the interfacial width narrowing by NR, rather than domain swelling as in Figure 2B, since domain swelling can occur from both an increase of χ and the presence of IL in a domain block. As the IL content increases, the T_g of the PMMA block steadily decreases due to the presence of IL, but at a much slower rate;[55] however, a small change in IL is sufficient to induce a large change in χ on top of enhanced mobility for rapid ordering of the BCP.

While the addition of IL to as-cast films produced relatively ordered and swollen domains, we next show the effect of solvent annealing by DIA in a neutral solvent mixture on domain ordering and spacing. In Figure 3, the AFM surface morphology of the same type of as-cast films presented so far in Figure 1 was annealed by the method of direct immersion annealing (DIA) for BCP ordering.[22] Figure 3 shows the results by immersion in a DIA solvent mixture of 3:1, heptane to toluene for 30 min. The surface profile looks more developed with longer-range order, characterized later in terms of the orientational correlational length. The AFM surface morphology images show a sharper contrast between the phases. This sharply contrasting result comes from the fact that the PMMA block subdomain is plasticized by IL and therefore the interfacial width w, expressed as $w = \frac{2a}{\sqrt{6\chi}}$ in the strong segregation limit (SSL),[54] decreases since IL increases the χ. DIA solvent also influences χ according to Zeman[56] relationships, $\chi_{\text{eff}} = \frac{(\chi_{1s} - \chi_{2s})^2}{(\delta_1 + \delta_2 - 2\delta_s)^2}\frac{RT}{v}$, where $(\chi_{1s} - \chi_{2s})$ is the difference in χ of the blocks of the solvent, R is the universal gas constant, v is the molar volume, T is the temperature, and δ is the solubility parameter. With the increase in χ_{eff}, it is therefore expected that the interfacial width decreases. In the inset, the GISAXS profile shows that the perpendicular component of the peak has been dramatically enhanced. The

https://doi.org/10.1021/acs.macromol.1c01305
Macromolecules 2021, 54, 8512–8525

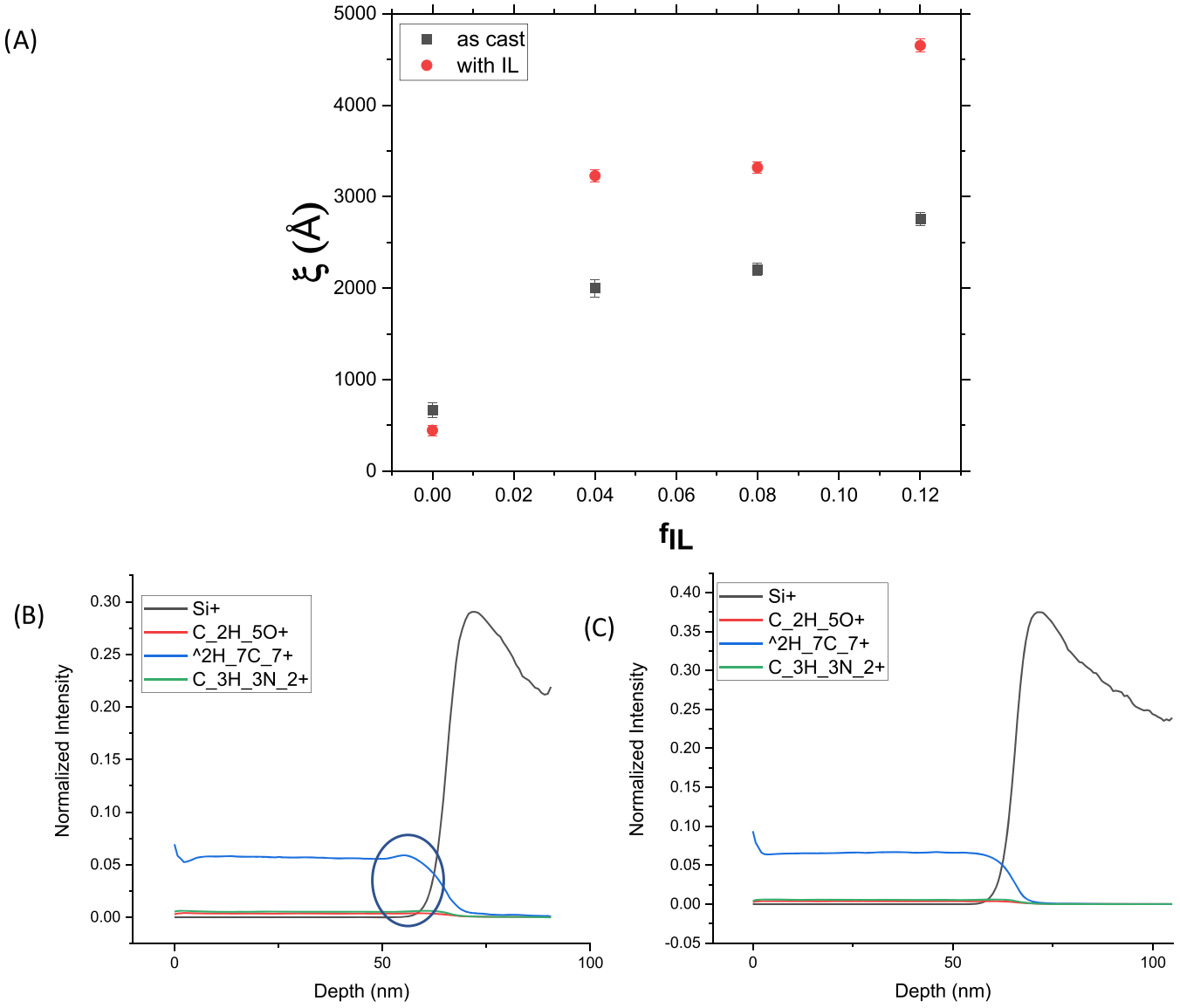

Figure 5. (A) Orientational correlation length obtained from the GISAXS of as-cast and DIA films. (B) ToF-SIMS profile of PS-PMMA 33k−33k films of about 60−70 nm after DIA with a 1:3 toluene to heptane mixture with (a) no IL and (C) with 10 mass % IL. It can be seen without IL that the structure is not entirely vertical, and a small PS-PMMA domain segregation is apparent. It is, however, absent in the IL film. Near the surface, there is slightly more PS in both cases of about 6 nm width, which is the surface undulation that arises from PS-bumps above PMMA. This may purely be a surface roughness effect.

integrated line-cut profile shows that the first-order peak after DIA is enhanced. With no IL, the peak has not much evolved, staying almost the same as earlier in the as-cast films. However, with IL, the first-order peak and the higher-order peak are sharper, as seen in the inset of Figure 3.

In Figure 4A, the line-cut profile from the GISAXS after DIA and the first-order peak occurs at 30.2 nm for no IL and 47.6 nm at 4 mass % IL and 49.5 nm at 8 mass % IL, with the presence of higher-order peaks ($\sqrt{4}$, $\sqrt{9}$), and the profile is more pronounced than as-cast l-BCP films. Again, we notice a hump after the first-order peak, and it may be arising from the asymmetry of the system due to IL swelling of PMMA, suggesting that IL remains in the films. The domain structures have shrunk a little compared to the as-cast films. To explain this, we propose one of two possible reasons, either that the rapid evaporation of DIA solvents leads to chain shrinkage or that some IL is lost to the DIA solvent. However, the IL used here is insoluble in both solvents of the DIA mixture at all proportions as per our observation. We note that, like in the previous analysis, it is clear that the effect of IL in the swelling of the domains also occurs in DIA-annealed samples. Notably, the domain length from the surface AFM profile and the GISAXS bulk film measurement (Figure 4B) line-cuts is almost the same.

The orientational correlation length ξ is a measure of the statistical robustness of the grain size of the ordering obtained from the peak of the GISAXS. The full width at half-maximum (FWHM) of the peaks from the GISAXS line-cut profiles can be used to calculate ξ to quantify the positional and orientational order using the Scherrer analysis,

$$\xi = \frac{2\pi k}{\Delta q}$$

where Δq can be expressed as,

https://doi.org/10.1021/acs.macromol.1c01305
Macromolecules 2021, 54, 8512−8525

$$\Delta q = \frac{4\pi}{\lambda}\cos(\theta)\frac{B}{2}$$

where 2θ is the scattering angle, B is the width of the Bragg peak (fwhm), λ is the wavelength of X-rays used (1.6868 Å), and K is the Scherrer constant (≈0.94).[57] Figure 5A shows ξ obtained from the as-cast films and after DIA. It is seen that overall, the statistical and positional ordering of the DIA systems is higher than the as-cast films. Significant improvement in ξ is noticeable in the 4 and 8% IL systems after DIA, with about a 50% increase in grain size. The swelling ratio determines the mobility of the BCP, and a higher swelling ratio generally indicates a higher polymer−solvent interaction and higher mobility if the swelling time window is limited. The accurate determination of the swelling ratio requires in situ measurement of the film thickness in the solvent environment, and due to experimental limitations, such studies could not be performed here. However, it is reported in the literature that PS can swell up to a ratio of 2 in the presence of toluene,[21] and PS-PMMA has been shown to have an optimum swelling ratio of 1.5−1.9 in the presence of acetone and heptane having a 0.2−0.4 acetone fraction.[22] Based on those data, it can be predicted that the BCP swells to a ratio of 1.5−2.0 when the fraction of toluene is between 0.3 and 1.0 in the solvent mixture. As more solvent incorporates into the BCP, there is enahnced mobility and thermodynamic driving force, i.e., larger ($\chi_{BCP/IL\text{-}tol}$), allowing rapid ordering with fewer defects, along with greater order formation with higher domain alignment. However, it is emphasized that annealing too long in any solvent environment can lead to autophobic dewetting. Indeed, we find that if annealing is continued over 90 min the films ultimately start to dewet.

To further demonstrate that DIA with IL has a specific advantage in the creation of the perpendicular orientation, ToF-SIMS was performed on a sample containing no IL or 10 mass % IL after DIA. From the Tof-SIMS profile in Figure 5B,C, we see that near the substrate surface in films without IL, a PMMA segregation layer is present that is absent in the IL-containing film. In fact, with IL, the profile is more uniform throughout the entirety of the film. According to Zeeman,[56] in the presence of a solvent, the interaction of the solvents with blocks and the presence of IL both can cause a significant increase in χ and a narrower interface. This shapened interface, coupled with the near-neutral environment provided by the solvent and IL, results in an enhanced vertical structure obtained after DIA. Figure S6 in the Supporting Information shows the same films etched using a 193 nm UV radiation to remove between 35 and 40 nm of the films. It is seen that the order propagates through the film in the IL-containing films, and there is almost no order in the no IL-containing films.

The attainment of significant vertical ordering in a low M_w PS-PMMA system is not very easy, as it readily forms a parallel structure since the substrate-driving force and polymer mobility can be very high. We have cast the lamellar PS-PMMA, 10k−10k films on the silicon substrate and neutral silicon substrate, attained using a thin layer of PS-*r*-PMMA (0.58 PS ratio) on the silicon substrate. Our findings suggest that adding too much IL (>25%) readily forms a parallel lamellar structure even in as-cast films (and morphological transformation occurs at about 40−50% IL by mass). Once the parallel lamellae have formed, these structures cannot readily transition back to vertical lamellae because of a large kinetic barrier. Applying DIA in a near-neutral solvent using these films is not useful, as vertical lamellae are in a less thermodynamically stable state. Thermally annealing these films also readily converts them to parallel lamellae even in short times. The as-cast films on silicon and neutral surface are seen in Figure S8. It is seen that as IL is added, some vertical lamellae are formed even in the as-cast films, although not very pronounced. After DIA for 30 min in the toluene: heptane 1:3 mixture (Figure S9), vertical lamellae are formed in the 5 and 10% IL films on silicon and neutral substrates. A very short-range vertical structure also arises in BCP films with no IL-additive films, but the range appears to significantly improve when the IL is added. On the silicon or a neutral substrate (Figure S9F), 10% IL has the best long-range vertical order with a domain size of 23 nm and a half-domain size of 11.5 nm, which includes the swelling. The stable thermodynamic structure of this polymer system is about 18 nm using SSL, similar to that obtained in these films without IL after DIA (Figure S9A,D).

In the Supporting Information, Figures S4 and S5 show a large enhancement of orientation in parallel lamellar films of high to very high M_w PS-PMMA (100k and 128k), obtained using DIA with the same solvent mixture and a small amount of selective solvent acetone. The acetone, being selective to PMMA block, allows the parallel lamellar organization. Overall, DIA with IL shows an improved long-range order of vertically or parallel oriented lamellae with lower defect density, according to the solvent environment, i.e., neutral solvent gives long-range vertical lamellae, and selective solvent allows parallel lamellae formation over a large region of the film with reduced domain length and an interfacial width in a very short time compared to thermal annealing.

SVA with IL for Suppression of Dewetting and Improvement of Long-Range Ordering. Although in DIA, some IL may be removed in the solvent, in SVA, the IL stays in the film, and the film will absorb an equilibrium amount of the solvent vapor that can interact with the film. Notably, very few studies of the SVA of the PS-PMMA system have been explored in the literature. Peng et al. performed an earlier study with acetone vapor with symmetric PS-PMMA with a PMMA homopolymer for a limited time exposure to (<5 h) SVA and observed perpendicular cylindrical morphology on the surface with SEM.[58] Severe dewetting of PS-PMMA films, annealed with SVA using acetone, on the silicon surface was also first noticed by Peng et al.[59] They subsequently investigated SVA of PS-PMMA using neutral solvent THF, PS-selective solvent CS_2, and the PMMA-selective acetone solvent with limited time of annealing. They found a terraced structure in a neutral solvent with no robust ordering, dewetting in PMMA-selective solvent, and PS-selective solvent attained a disordered micellar structure.[60] Gong et al. also observed the rapid dewetting of the PS-PMMA film with the THF solvent and combined SVA (for 1 h) to attain a metastable structure followed by thermal annealing to attain better ordering.[61] Thus, it is well-understood that PS-PMMA films can easily dewet when good solvent vapors are absorbed in the film, especially if annealing is continued for a longer time to attain the desired complete ordering. The reason may be because a good solvent for both blocks induces high swelling and mobility that leads to dewetting in the SVA environment since mostly good solvents are absorbed in the films during SVA.

It is nonetheless technologically useful to order BCP films using an SVA system since SVA can potentially order BCPs faster than thermal melt annealing with lower defect density and attain long-range ordering. In this context, longer annealing times (15−24 h) can typically aid in yielding highly ordered and defect-free self-assembly of the BCP. We show here that the

https://doi.org/10.1021/acs.macromol.1c01305
Macromolecules 2021, 54, 8512−8525

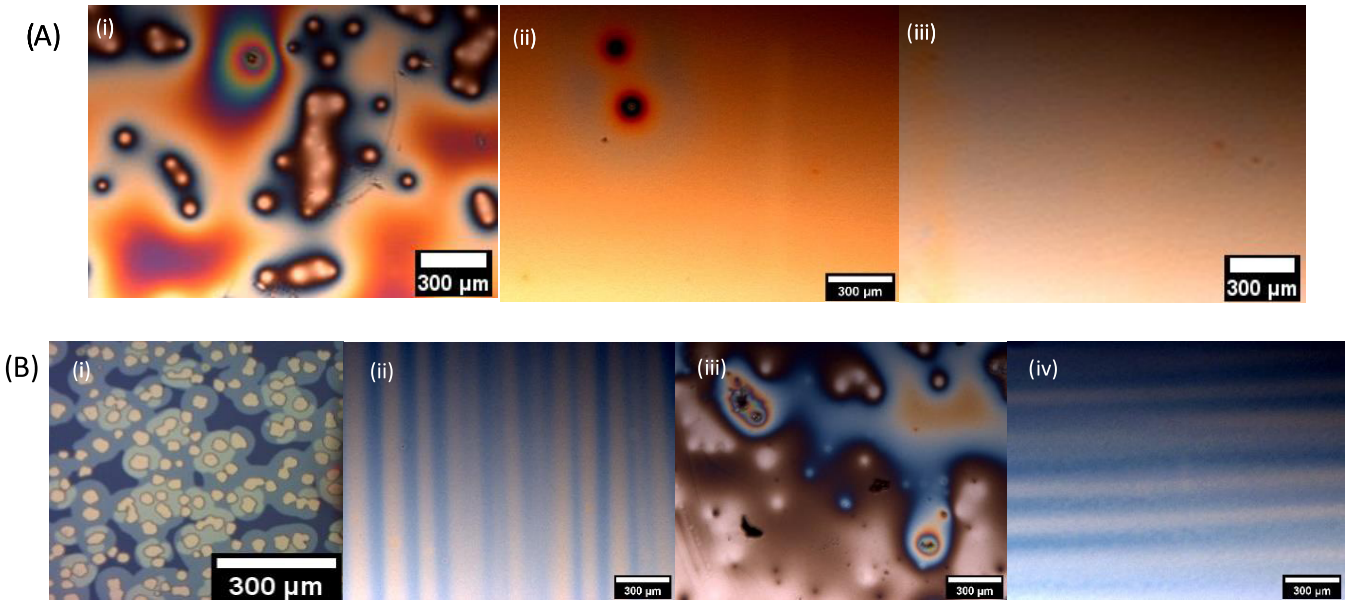

Figure 6. (A) Optical microscopy image of SVA for 15 h in toluene and heptane mixture in PS-PMMA (55−22): (i) highly dewet film with no IL, (ii) stabilization with 5% IL, and (iii) better stabilization with 10 mass % IL. (B) Optical microscopy image of SVA for 15 h: (i) highly dewet PS-PMMA (55−22) film SVA using toluene, (ii) stabilization of film against dewetting using 10 mass % IL toluene for SVA, (iii) dewet using no IL using acetone SVA, and (iv) stabilization against dewetting using 10 mass % IL using acetone for SVA.

presence of IL in the as-cast BCP films can induce ordering in low χ polymer systems, such as PS-PMMA, without dewetting for longer annealing times using SVA to attain complete ordering with very low defect density and long-range order using neutral and pure solvent systems.

Figure 6 shows the optical microscope image for films of PS-PMMA (55k−22k) with a cylindrical morphological structure (c-BCP) of thickness between 150 nm and 160 nm on the surface of a silicon wafer after SVA. The images demonstrate that adding IL helps to suppress dewetting in the limit of longer annealing times of 15 h to attain a defect-free robust self-assembled structure. It can be seen in Figure 6A(i−iii) that adding IL suppresses dewetting when ordered using a neutral SVA solvent having a composition of 3:1 heptane to toluene ratio. The SVA was performed in a closed chamber at room temperature using the normal vapor pressure of the solvent mixture. The vapor pressure of heptane at room temperature is 46 mm Hg[62] and that of toluene at room temperature is 28.4 mm Hg at 25 °C.[63] It is expected, however, that despite toluene having a lower vapor pressure and composition in the solvent mixture, more toluene is absorbed in the films compared to heptane since toluene is a good solvent for both the polymer blocks and heptane is a poor solvent. Our finding also suggests that the IL used in this study is entirely insoluble in both toluene and heptane. It is known that the solvent system can swell polymer films significantly and induce chain mobility that can potentially enable dewetting in the films, which is counteracted by the IL due to enhancement of χ and thereby stiffer interfaces that impart more resiliency to the film from weaker dewetting forces, coupled with reduced diffusivity arising from $D \sim \exp(-\alpha\chi)$ for a fixed polymer mass.

Figure 7 shows the AFM image of the SVA-ordered films using the earlier DIA, neutral solvent mixture (3:1 heptane to toluene). Since the films without IL were dewet, therefore the AFM image of those films could not be collected. The film in Figure 7A contains a stable 2 mass % IL, so this shows that 2 mass % IL is sufficient to suppress dewetting in 15 h of SVA using the neutral solvent mixture. The order, however, is not very long range and the BCP film appears to have a lot of defects present. A much higher long-range ordering was obtained using 10 mass % IL (Figure 7B) when compared to that using the 2 mass % IL, which is remarkable.

The domain length in this film obtained from AFM is 37−41 nm from the surface profile of Figure 7A,B. From the GISAXS first-order peak, the length scale is about 36 nm. Since cylindrical films are arranged in a hexagonal pattern, therefore there are two in-plane domain lengths, as illustrated in Figure S2. Thus, the domain length has to be multiplied by $2/\sqrt{3}$ to attain the domain length, which is about 41.6 nm in the 2 mass % IL and about 43.9 nm in the 10 mass % IL. This shows that the IL has caused some swelling to the domain length. We hypothesize that this has to do with the expansion of the film in the in-plane direction parallel to the silicon substrate being not readily accessible due to the pinning effect of the film to the substrate. Therefore, horizontal swelling is limited and stays near to the equilibrium domain spacing even with the IL.

Moreover, from the GISAXS image in Figure 7, the first-order peak and the second-order peak are present and become more oriented and intense from 10 mass % IL compared to those from 2 mass % IL. In the cylindrical morphology, when a mixed morphology of perpendicular and parallel cylinders is present, the first-order peak usually splits into two peaks.[57] As the first-order peak did not split, it suggests that the cylinder morphology is entirely vertical. (A sharp peak is present at around $q_y = 0.02$, which we attribute to the detector electronic pixel noise and not the films itself.) As before, the bulk GISAXS and surface AFM domain structures mostly correspond well dimensionally to each other. It is also quite interesting to notice that the films with IL are stable for up to 24 h as investigated. The dewetting phenomenon can arise because good solvents create mobility in the polymer blocks and cause autophobic dewetting (film dewets a monolayer of its own kind due to entropic immiscibility) when annealing is continued for a longer time. However, in a short period, films may be stable as only short

https://doi.org/10.1021/acs.macromol.1c01305
Macromolecules 2021, 54, 8512−8525

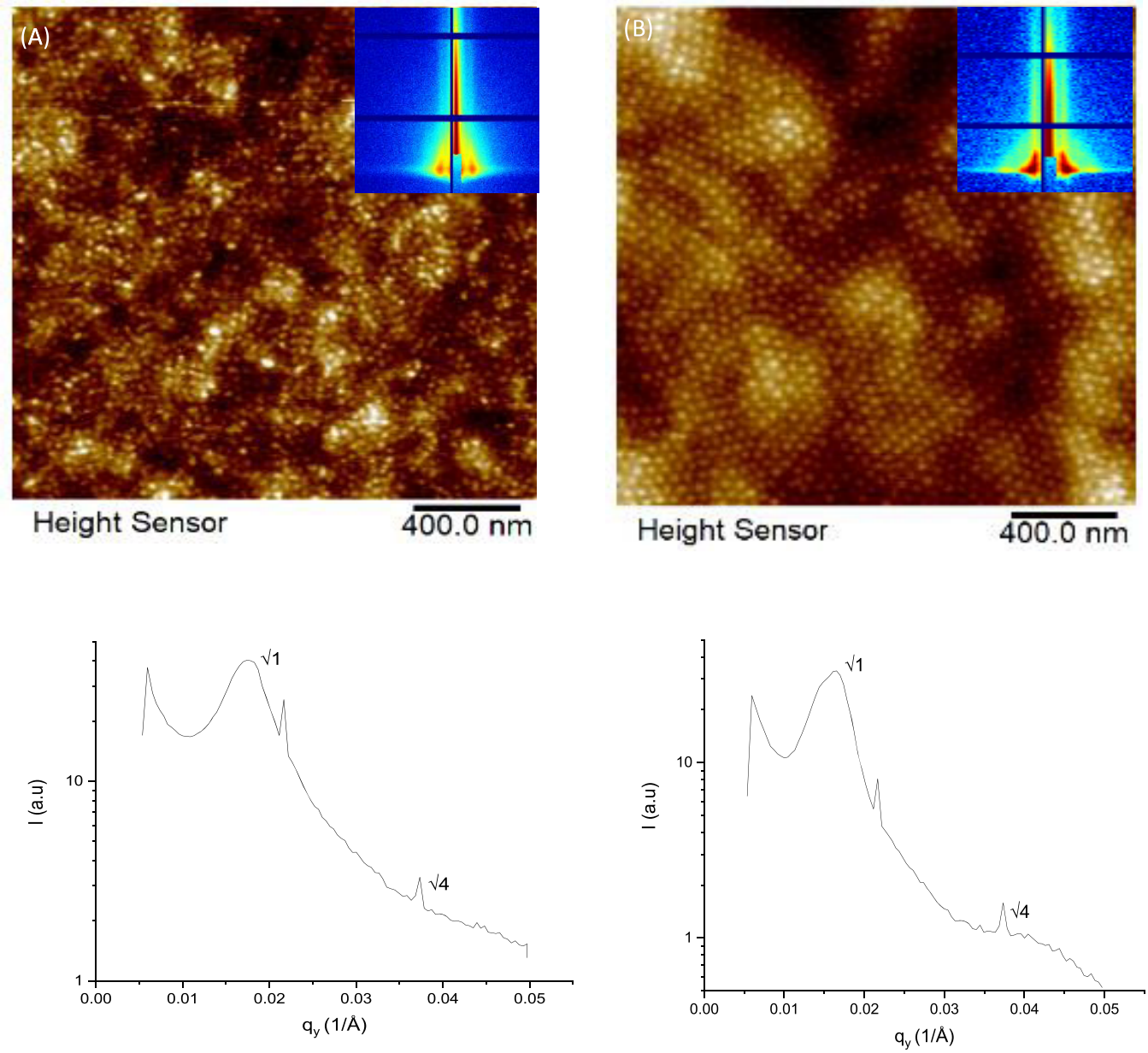

Figure 7. AFM and GISAXS of SVA of the cylindrical PS-PMMA (55k−22k) films using toluene and heptane for 15 h with (A) 2 mass % IL and (B) 10 mass % IL.

segments of the polymer relax and rearrange to a thermodynamically stable form. In a more extended time, the motion of the entire chain leads to dewetting. Without the IL, the movement of the chain is disordered with high mobility in the presence of good solvents leading to complete dewetting before complete ordering transition can occur. However, with IL, the motion of the polymer chains is reduced and effectively stiffens due to the formation of a highly ordered interfacial PS-PMMA structure, so the film dewetting is inhibited even when the film is annealed for 24 h.

Since the IL makes the BCP film morphology more stable, we next explored if pure solvent-based SVA, like pure toluene (slightly PS-selective) or acetone (PMMA-selective), leads to dewetting in films containing IL. After 15 h of SVA, we observed that the films containing no IL dewet completely, while those containing 10 mass % IL were stable. Films containing a smaller amount of IL, i.e., 2 and 5 mass % IL, also dewet. We found that films containing 10 mass % IL or higher (up to 20 mass %) were stable. We note that a pure IL film that is flow-coated on the silicon substrate tends to dewet the substrate, so this is not due to the enhanced intrinsic wettability of excess IL on the substrate. Also, the films demonstrated superior ordering, with lower defect density and long-range order, as can be seen in Figure 8A,B. Very long-range order is observed from the AFM image in Figure 8A for the SVA of c-BCP films using only toluene vapors at room temperature in a closed chamber. It is observed that if there is an elevation change (Figure 8A) in the film surface, there is a change in the direction of the ordering propagation, with orders that are significantly more oriented compared to what can usually be attained with these films. Since height directly affects the commensurability condition in BCP films, therefore a change in direction is observed with a change of height. These c-BCP films (PS-PMMA 55k−22k) have a high PS M_w and are not easy to order using thermal annealing as seen

https://doi.org/10.1021/acs.macromol.1c01305
Macromolecules 2021, 54, 8512−8525

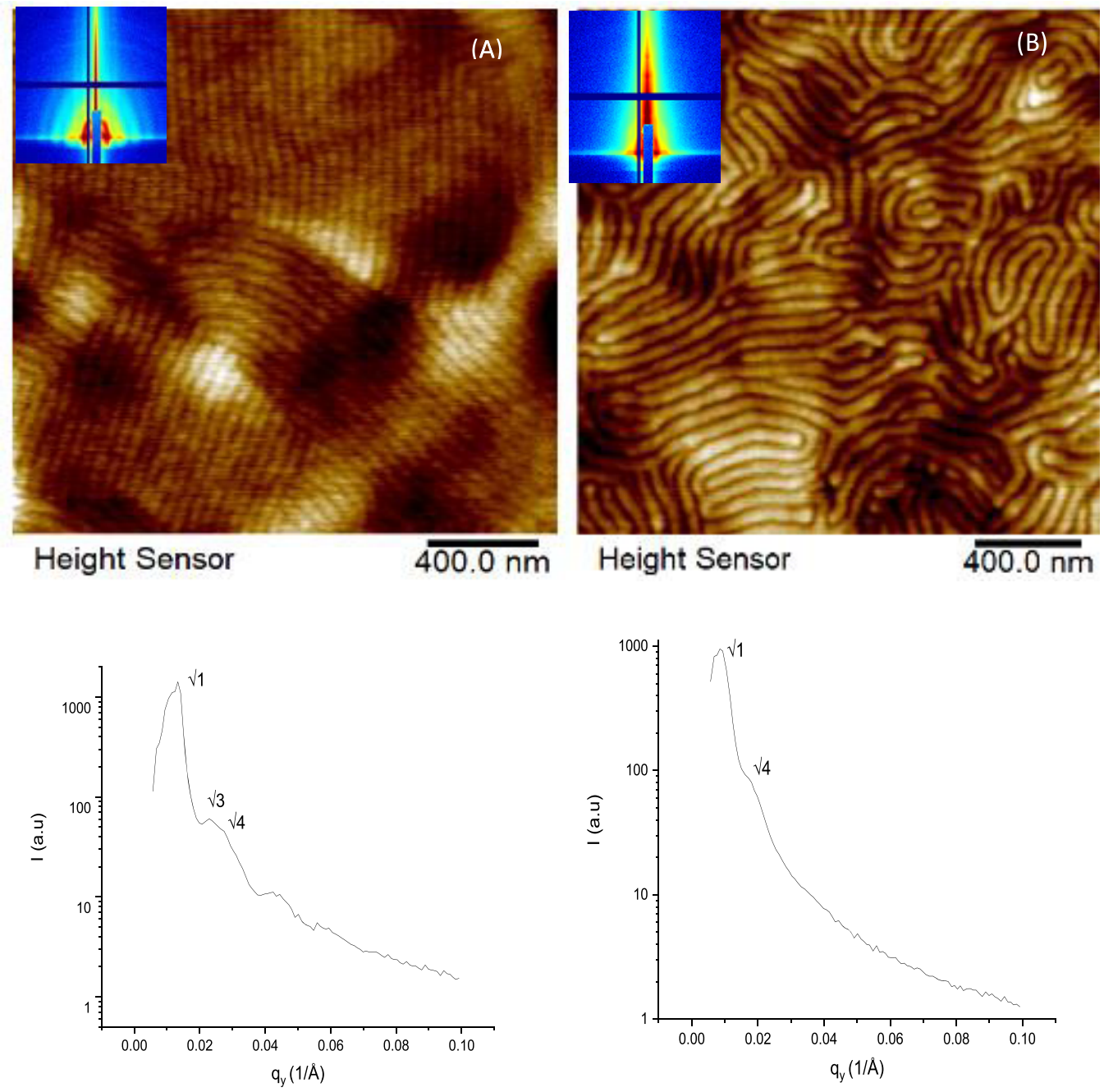

Figure 8. AFM and GISAXS of SVA of the cylindrical PS-*b*-PMMA (55k−22k) films for (A) 15 h in toluene with 10 mass % IL and (B) 15 h using acetone with 10 mass % IL.

in Figure S7; even after annealing at 170 °C for 24 h with or without IL for films of thickness (70−80) nm, some metastable surface ordering is present, with no significant bulk order confirmed by UV ablation of the films and AFM.

Figure 8B shows the AFM image of the SVA with acetone for the PS-PMMA cylindrical structure (55k−22k) with 10 mass % IL. Again, at lower IL fractions, the film dewets for a longer annealing time with acetone. Cylinders (transitioned to lamellar confirmed from GISAXS) arranged parallel to the substrate are obtained here with proper identical ordering. The domain length from the AFM is 65 nm, which is high compared to the thermodynamically stable 41 nm for this polymer without IL. Although films were rapidly dried, the IL is completely soluble in acetone, and therefore, this could be due to some retention of solvent in the system. However, such significant swelling also indicates a large enhancement of the χ parameter ($L_0 \sim \chi^{1/6}$). In Figure 8, the GISAXS corresponding to the toluene SVA is seen in Figure 8A, and acetone SVA is seen in Figure 8B. The first-order peak in both is very strong, confirming the robust ordering present in the system. The AFM and GISAXS domain length mostly match up here, as seen in Table 1. The $\sqrt{3}$ and $\sqrt{4}$ peaks present in cylindrical systems (Figure 8A) are also seen, although $\sqrt{3}$ peak with acetone (Figure 8B) is not very clear or not present. This suggests that a morphological transition from cylinder to a lamellar structure occurred in the presence of acetone since acetone/IL causes more swelling in the smaller PMMA block leading to morphological transition. The robustness of the ordering reveals that SVA with IL makes PS-PMMA

https://doi.org/10.1021/acs.macromol.1c01305
Macromolecules 2021, 54, 8512−8525

Table 1. Domain Length from AFM and GISAXS and Theoretical Domain Length Obtained Using SSL Approximation for PS-PMMA 55k−22k

	AFM (nm)	GISAXS (nm)	theoretical (nm)
Figure 7A	37−39	41.6	41
Figure 7B	38−41	43.9	41
Figure 8A	47	47.6	41
Figure 8B	65	67.5	41

more processible with a higher range of ordering and improved thermodynamic properties for phase separation useful in many technological applications such as membranes and photonic materials currently being explored as future works.

CONCLUSIONS

We have thoroughly studied the enhancement of the vertical ordering in the PS-PMMA block copolymers with IL and solvent-based direct immersion annealing (DIA) and with the more established technique of solvent vapor annealing (SVA). The solvents can alter the thermodynamic properties of the block copolymer system and tune chain mobility to the extent that they can induce robust ordering before dewetting. A creative binary solvent mixture design for DIA with EMIM TFSI was shown to rapidly induce a vertical order in lamellae forming PS-PMMA block copolymer systems when annealed using DIA. The results were thoroughly validated using direct imaging, grazing scattering, UVO ablation, and real-time chemical depth analysis using secondary ion mass spectroscopy methods. They were shown to have longer-range order using grain size analysis in IL-containing DIA films. The IL establishes synergy to the binary solvent mixture of toluene and heptane to create a neutral solvent environment for the vertical microstructure of the BCP using the DIA and SVA methods. We have also shown that IL can suppress dewetting over longer annealing times using SVA and using pure solvents to attain long-range ordering in the systems that would otherwise dewet over longer annealing times. These findings are important as they can help achieve long-range order for many nanofunctional applications.

ASSOCIATED CONTENT

Supporting Information

The Supporting Information is available free of charge at https://pubs.acs.org/doi/10.1021/acs.macromol.1c01305.

Schematic of the experimental setup for the SVA and DIA experiments; both were done in a closed chamber at atmospheric temperature and pressure (Figure S1); schematic 3D arrangement of the cylindrical morphology structure when they order (Figure S2); neutron reflectivity data of the dPS-PMMA 19.5k−18.1k, annealed in selective DIA for 1 h with and without IL and their respective SLD profile (Figure S3); schematic arrangement of the ToF-SIMS methodology (Figure S4); enhanced parallel lamellar orientation obtained using high M_w lamellar dPS-PMMA (47.5k−51k) with a molecular weight of about ≈100k in a selective DIA bath characterized by ToF-SIMS (Figure S5); ToF-SIMS of very high M_w PS-PMMA (65k−62.5k) annealed using DIA in a selective DIA for 4−10 h (Figure S6); AFM surface profile of cylindrical PS-PMMA (55k−22k) using thermal annealing for 170 °C for 24 h for films of (70−80 nm) and after etching to remove about 40−45 nm (Figure S7); AFM image of the PS-PMMA (10k−10k) films of thickness 30−40 nm, as-cast using flow coating on a bare silicon substrate and neutral silicon substrate attained by coating a PS-*r*-PMMA polymer with a 0.58 molar fraction of PS (Figure S8); and AFM profile of the same films after DIA in (1:3) heptane and toluene volume ratio mixture for 30 min (Figure S9) (PDF)

AUTHOR INFORMATION

Corresponding Authors

Jack F. Douglas − *Materials Engineering Laboratory, National Institute of Standards and Technology, Gaithersburg, Maryland 20899, United States;* orcid.org/0000-0001-7290-2300; Email: jack.douglas@nist.gov

Alamgir Karim − *Department of Chemical and Biomolecular Engineering, University of Houston, Houston, Texas 77204, United States;* orcid.org/0000-0003-1302-9374; Email: akarim3@Central.UH.EDU

Authors

Ali Masud − *Department of Chemical and Biomolecular Engineering, University of Houston, Houston, Texas 77204, United States;* orcid.org/0000-0001-7619-4364

Wenjie Wu − *Department of Chemical and Biomolecular Engineering, University of Houston, Houston, Texas 77204, United States*

Maninderjeet Singh − *Department of Chemical and Biomolecular Engineering, University of Houston, Houston, Texas 77204, United States;* orcid.org/0000-0001-8891-8454

Wafa Tonny − *Department of Chemical and Biomolecular Engineering, University of Houston, Houston, Texas 77204, United States*

Ali Ammar − *Department of Chemical and Biomolecular Engineering, University of Houston, Houston, Texas 77204, United States*

Kshitij Sharma − *Department of Chemical and Biomolecular Engineering, University of Houston, Houston, Texas 77204, United States*

Joseph W. Strzalka − *X-Ray Science Division, Argonne National Laboratory, Lemont, Illinois 60439, United States;* orcid.org/0000-0003-4619-8932

Tanguy Terlier − *Shared Equipment Authority, Rice University, Houston, Texas 77005, United States*

Complete contact information is available at: https://pubs.acs.org/10.1021/acs.macromol.1c01305

Notes

Certain commercial materials and equipment are identified to adequately specify the experimental procedure. In no case does such identification imply recommendation by the National Institute of Standards and Technology nor does it imply that the material or equipment identified is necessarily the best available for this purpose.

The authors declare no competing financial interest.

ACKNOWLEDGMENTS

A.K. would like to acknowledge the funding supported by the National Science Foundation (NSF) via Grant DMR-1905996. This research used resources of the Advanced Photon Source, a U.S. Department of Energy (DOE) Office of Science User Facility operated for the DOE Office of Science by Argonne National Laboratory under Contract No. DE-AC02-

https://doi.org/10.1021/acs.macromol.1c01305
Macromolecules 2021, 54, 8512−8525

06CH11357. ToF-SIMS analyses were carried out with support provided by the National Science Foundation CBET-1626418. This work was conducted, in part, using resources of the Shared Equipment Authority at Rice University. The authors also acknowledge Guangcui Yuan and Sushil K. Satija at the NIST Center for Neutron Research and the neutron reflection beam time made available for this study.

REFERENCES

(1) Berry, B. C.; Singh, G.; Kim, H. C.; Karim, A. Highly Aligned Block Copolymer Thin Films by Synergistic Coupling of Static Graphoepitaxy and Dynamic Thermal Annealing Fields. *ACS Macro Lett.* **2013**, *2*, 346−350.
(2) Singh, M.; Apata, I. E.; Samant, S.; Wu, W.; Tawade, B. V.; Pradhan, N.; Raghavan, D.; Karim, A. Nanoscale Strategies to Enhance the Energy Storage Capacity of Polymeric Dielectric Capacitors: Review of Recent Advances. *Polym. Rev.* **2021**, 1−50.
(3) Ye, C.; Sun, Y.; Karim, A.; Vogt, B. D. Extending Dynamic Range of Block Copolymer Ordering with Rotational Cold Zone Annealing (RCZA) and Ionic Liquids. *Macromolecules* **2015**, *48*, 7567−7573.
(4) Lin, Y. H.; Yager, K. G.; Stewart, B.; Verduzco, R. Lamellar and Liquid Crystal Ordering in Solvent-Annealed All-Conjugated Block Copolymers. *Soft Matter* **2014**, *10*, 3817−3825.
(5) Weber, R. L.; Ye, Y.; Schmitt, A. L.; Banik, S. M.; Elabd, Y. A.; Mahanthappa, M. K. Effect of Nanoscale Morphology on the Conductivity of Polymerized Ionic Liquid Block Copolymers. *Macromolecules* **2011**, *44*, 5727−5735.
(6) Zhang, S.; Lee, K. H.; Frisbie, C. D.; Lodge, T. P. Ionic Conductivity, Capacitance, and Viscoelastic Properties of Block Copolymer-Based Ion Gels. *Macromolecules* **2011**, *44*, 940−949.
(7) Samant, S. P.; Grabowski, C. A.; Kisslinger, K.; Yager, K. G.; Yuan, G.; Satija, S. K.; Durstock, M. F.; Raghavan, D.; Karim, A. Directed Self-Assembly of Block Copolymers for High Breakdown Strength Polymer Film Capacitors. *ACS Appl. Mater. Interfaces* **2016**, *8*, 7966−7976.
(8) Bates, F. S.; Fredrickson, G. H. Block Copolymer Thermodynamics: Theory and Experiment. *Annu. Rev. Phys. Chem.* **1990**, *41*, 525−557.
(9) Longanecker, M.; Modi, A.; Dobrynin, A.; Kim, S.; Yuan, G.; Jones, R.; Satija, S.; Bang, J.; Karim, A. Reduced Domain Size and Interfacial Width in Fast Ordering Nanofilled Block Copolymer Films by Direct Immersion Annealing. *Macromolecules* **2016**, *49*, 8563−8571.
(10) Sinturel, C.; Bates, F. S.; Hillmyer, M. A. High χ-Low N Block Polymers: How Far Can We Go? *ACS Macro Lett.* **2015**, *4*, 1044−1050.
(11) Ruiz, R.; Dobisz, E.; Albrecht, T. R. Rectangular Patterns Using Block Copolymer Directed Assembly for High Bit Aspect Ratio Patterned Media. *ACS Nano* **2011**, *5*, 79−84.
(12) Singh, M.; Wu, W.; Basutkar, M. N.; Strzalka, J.; Al-Enizi, A. M.; Douglas, J. F.; Karim, A. Ultra-Fast Vertical Ordering of Lamellar Block Copolymer Films on Unmodified Substrates. *Macromolecules* **2021**, *54*, 1564−1573.
(13) Wu, W.; Singh, M.; Masud, A.; Wang, X.; Nallapaneni, A.; Xiao, Z.; Zhai, Y.; Wang, Z.; Terlier, T.; Bleuel, M.; et al. Control of Phase Morphology of Binary Polymer Grafted Nanoparticle Blend Films via Direct Immersion Annealing. *ACS Nano* **2021**, *15*, 12042−12056.
(14) Miller-Chou, B. A.; Koenig, J. L. Dissolution of Symmetric Diblock Copolymers with Neutral Solvents, a Selective Solvent, a Nonsolvent, and Mixtures of a Solvent and Nonsolvent Monitored by FT-IR Imaging. *Macromolecules* **2003**, *36*, 4851−4861.
(15) Chaudhari, A.; Ghoshal, T.; Shaw, M. T.; Borah, D.; Chaudhari, A.; Ghoshal, T.; Shaw, M. T.; Cummins, C.; Holmes, J. D.; Morris, M. A. Formation of sub-7 nm feature size PS-b-P4VP block copolymer structures by solvent vapour process. *Proc. SPIE* **2018**, *9051*, No. 905110-1.
(16) Lundy, R.; Flynn, S. P.; Cummins, C.; Kelleher, S. M.; Collins, M. N.; Dalton, E.; Daniels, S.; Morris, A.; Enright, R. Controlled Solvent Vapor Annealing of a High v Block Copolymer Thin Film. *Phys. Chem. Chem. Phys.* **2017**, *19*, 2805−2815.
(17) Aissou, K.; Fleury, G.; Pecastaings, G.; Alnasser, T.; Goglio, G.; Hadziioannou, G. Hexagonal-to-Cubic Phase Transformation in Composite Thin Films Induced by FePt Nanoparticles Located at PS / PEO Interfaces. *Langmuir* **2011**, *27*, 14481−14488.
(18) O'Driscoll, S.; Demirel, G.; Farrell, R. A.; Fitzgerald, T. G.; Mahony, C. O.; Holmes, J. D.; Morris, M. A. The Morphology and Structure of PS-b-P4VP Block Copolymer Films by Solvent Annealing: Effect of the Solvent Parameter. *Polym. Adv. Technol.* **2011**, *22*, 915−923.
(19) Kim, E.; Park, S.; Han, Y.; Kim, T. Effect of Solvent Selectivity on Supramolecular Assemblies of Block Copolymer by Solvent-Vapor Annealing. *Polymer* **2018**, *150*, 214−222.
(20) Cavicchi, K. A.; Lodge, T. P. Anisotropic Self-Diffusion in Block Copolymer Cylinders. *Macromolecules* **2004**, *37*, 6004−6012.
(21) Park, W. I.; Kim, J. M.; Jeong, J. W.; Jung, Y. S. Deep-Nanoscale Pattern Engineering by Immersion-Induced Self-Assembly. *ACS Nano* **2014**, *8*, 10009−10018.
(22) Modi, A.; Bhaway, S. M.; Vogt, B. D.; Douglas, J. F.; Al-enizi, A.; Elzatahry, A.; Sharma, A.; Karim, A. Direct Immersion Annealing of Thin Block Copolymer Films. *ACS Appl. Mater. Interfaces* **2015**, *7*, 21639−21645.
(23) Ye, Y.-S.; Rick, J.; Hwang, B.-J. Ionic Liquid Polymer Electrolytes. *J. Mater. Chem. A* **2013**, *1*, 2719−2743.
(24) Bennett, T. M.; Pei, K.; Cheng, H.-H.; Thurecht, K. J.; Jack, K. S.; Blakey, I. Can Ionic Liquid Additives Be Used to Extend the Scope of Poly(Styrene)-Block-Poly(Methyl Methacrylate) for Directed Self-Assembly? *J. Micro/Nanolithogr., MEMS, MOEMS* **2014**, *13*, No. 031304.
(25) Bennett, T.; Pei, K.; Cheng, H.-H.; Thurecht, K. J.; Jack, K. S.; Blakey, I. Extending the Scope of Poly(Styrene)-Block-Poly(Methyl Methacrylate) for Directed Self-Assembly. In *Alternative Lithographic Technologies VI*; International Society for Optics and Photonics, 2014; Vol. *9049*, p 90490R.
(26) Chen, X.; Zhou, C.; Chen, S.; Craig, G. S. W.; Rincon-delgadillo, P.; Dazai, T.; Miyagi, K.; Maehashi, T.; Yamazaki, A.; Gronheid, R.; et al. Ionic Liquids as Additives to Polystyrene-b-Poly (Methyl Methacrylate) Enabling Directed Self-Assembly of Patterns with Sub-10 Nm Features. *ACS Appl. Mater. Interfaces* **2018**, *10*, 16747−16759.
(27) Bhadauriya, S.; Wang, X.; Nallapaneni, A.; Masud, A.; Wang, Z.; Lee, J.; Bockstaller, M. R.; Al-Enizi, A. M.; Camp, C. H., Jr; Stafford, C. M.; et al. Observation of General Entropy−Enthalpy Compensation Effect in the Relaxation of Wrinkled Polymer Nanocomposite Films. *Nano Lett.* **2021**, *21*, 1274−1281.
(28) Samant, S.; Basutkar, M.; Singh, M.; Masud, A.; Grabowski, C. A.; Kisslinger, K.; Strzalka, J.; Yuan, G.; Satija, S.; Apata, I.; et al. Effect of Molecular Weight and Layer Thickness on the Dielectric Breakdown Strength of Neat and Homopolymer Swollen Lamellar Block Copolymer Films. *ACS Appl. Polym. Mater.* **2020**, *2*, 3072−3083.
(29) Masud, A.; Longanecker, M.; Bhadauriya, S.; Singh, M.; Wu, W.; Sharma, K.; Terlier, T.; Al-Enizi, A. M.; Satija, S.; Douglas, J. F.; et al. Ionic Liquid Enhanced Parallel Lamellar Ordering in Block Copolymer Films. *Macromolecules* **2021**, *54*, 4531−4545.
(30) This Article Identifies Certain Commercial Materials, Equipment, or Instruments to Specify Experimental Procedures. Such Identification Implies Neither Recommendation or Endorsement by the National Institute of Standards and Technology.
(31) Jiang, Z. GIXSGUI: A MATLAB Toolbox for Grazing-Incidence X-Ray Scattering Data Visualization and Reduction, and Indexing of Buried Three-Dimensional Periodic Nanostructured Films. *J. Appl. Crystallogr.* **2015**, *48*, 917−926.
(32) Kienzle, P. A.; O'Donovan, K. V.; Ankner, J. F.; Berk, N. F.; Majkrzak, C. F. *NCNR Reflectometry Software*; NIST, 2006.
(33) Basutkar, M. N.; Samant, S.; Strzalka, J.; Yager, K. G.; Singh, G.; Karim, A. Through-Thickness Vertically Ordered Lamellar Block Copolymer Thin Films on Unmodified Quartz with Cold Zone Annealing. *Nano Lett.* **2017**, *17*, 7814−7823.
(34) Wang, H. S.; Kim, K. H.; Bang, J. Thermal Approaches to Perpendicular Block Copolymer Microdomains in Thin Films: A

https://doi.org/10.1021/acs.macromol.1c01305
Macromolecules 2021, 54, 8512−8525

Review and Appraisal. *Macromol. Rapid Commun.* **2019**, *40*, No. 1800728.
(35) Harris, M.; Appel, G.; Ade, H. Surface Morphology of Annealed Polystyrene and Poly (Methyl Methacrylate) Thin Film Blends and Bilayers. *Macromolecules* **2003**, *36*, 3307−3314.
(36) Black, C. T.; Ruiz, R.; Breyta, G.; Cheng, J. Y.; Colburn, M. E.; Guarini, K. W.; Zhang, Y.; Heights, Y. Polymer Self Assembly in Semiconductor Microelectronics. *IBM J. Res. Dev.* **2007**, *51*, 605−633.
(37) Xu, T.; Hawker, C. J.; Russell, T. P. Interfacial Interaction Dependence of Microdomain Orientation in Diblock Copolymer Thin Films. *Macromolecules* **2005**, *38*, 2802−2805.
(38) Maher, M. J.; Self, J. L.; Stasiak, P.; Blachut, G.; Ellison, C. J.; Matsen, M. W.; Bates, C. M.; Willson, C. G. Structure, Stability, and Reorganization of 0.5 L0Topography in Block Copolymer Thin Films. *ACS Nano* **2016**, *10*, 10152−10160.
(39) Maher, M. J.; Bates, C. M.; Blachut, G.; Sirard, S.; Self, J. L.; Carlson, M. C.; Dean, L. M.; Cushen, J. D.; Durand, W. J.; Hayes, C. O.; et al. Interfacial Design for Block Copolymer Thin Films. *Chem. Mater.* **2014**, *26*, 1471−1479.
(40) Zhang, X.; Douglas, J. F.; Satija, S.; Karim, A. Enhanced Vertical Ordering of Block Copolymer Films by Tuning Molecular RSC Advances Enhanced Vertical Ordering of Block Copolymer Films by Tuning Molecular Mass. *RSC Adv.* **2015**, *5*, 32307−32318.
(41) Huang, C.; Lodge, T. P. Self-Consistent Calculations of Block Copolymer Solution Phase Behavior. *Macromolecules* **1998**, *9297*, 3556−3565.
(42) Huang, E.; Pruzinsky, S.; Russell, T. P.; Mays, J.; Hawker, C. J. Neutrality Conditions for Block Copolymer Systems on Random Copolymer Brush Surfaces. *Macromolecules* **1999**, *32*, 5299−5303.
(43) Zhang, J.; Clark, M. B.; Wu, C.; Li, M.; Trefonas, P.; Hustad, P. D. Orientation Control in Thin Films of a High-χ Block Copolymer with a Surface Active Embedded Neutral Layer. *Nano Lett.* **2016**, *16*, 728−735.
(44) Ryu, D. Y.; Ham, S.; Kim, E.; Jeong, U.; Hawker, C. J.; Russell, T. P. Cylindrical Microdomain Orientation of PS-b-PMMA on the Balanced Interfacial Interactions: Composition Effect of Block Copolymers. *Macromolecules* **2009**, *42*, 4902−4906.
(45) Doerk, G. S.; Yager, K. G. Rapid Ordering in "Wet Brush" Block Copolymer/Homopolymer Ternary Blends. *ACS Nano* **2017**, *11*, 12326−12336.
(46) Han, J.; Zhai, Y.; Wang, Z.; Bleuel, M.; Liu, T.; Yin, R.; Wu, W.; Hakem, I. F.; Karim, A.; Matyjaszewski, K.; et al. Nanosized Organo-Silica Particles with "Built-in" Surface-Initiated Atom Transfer Radical Polymerization Capability as a Platform for Brush Particle Synthesis. *ACS Macro Lett.* **2020**, *9*, 1218−1223.
(47) Yoo, M.; Kim, S.; Jang, S. G.; Choi, S. H.; Yang, H.; Kramer, E. J.; Lee, W. B.; Kim, B. J.; Bang, J. Controlling the Orientation of Block Copolymer Thin Films Using Thermally-Stable Gold Nanoparticles with Tuned Surface Chemistry. *Macromolecules* **2011**, *44*, 9356−9365.
(48) Singh, G.; Yager, K. G.; Smilgies, D. M.; Kulkarni, M. M.; Bucknall, D. G.; Karim, A. Tuning Molecular Relaxation for Vertical Orientation in Cylindrical Block Copolymer Films via Sharp Dynamic Zone Annealing. *Macromolecules* **2012**, *45*, 7107−7117.
(49) Xu, T.; Zvelindovsky, A. V.; Sevink, G. J. A.; Lyakhova, K. S.; Jinnai, H.; Russell, T. P. Electric Field Alignment of Asymmetric Diblock Copolymer Thin Films. *Macromolecules* **2005**, *38*, 10788−10798.
(50) Bhadauriya, S.; Nallapaneni, A.; Wang, X.; Zhang, J.; Masud, A.; Bockstaller, M. R.; Al-Enizi, A. M.; Stafford, C. M.; Douglas, J. F.; Karim, A. Enhanced Resistance to Decay of Imprinted Nanopatterns in Thin Films by Bare Nanoparticles Compared to Polymer-Grafted Nanoparticles. *Nanoscale Adv.* **2021**, *3*, 5348−5354.
(51) Sinturel, C.; Morris, M.; Hillmyer, M. A. Solvent Vapor Annealing of Block Polymer Thin Films. *Macromolecules* **2013**, *46*, 5399−5415.
(52) Chu, C. J.; Cheng, M. H.; Chung, P. Y.; Chi, M. H.; Jeng, K. S.; Chen, J. T. Reversible Morphology Control of Three-Dimensional Block Copolymer Nanostructures by the Solvent-Annealing-Induced Wetting in Anodic Aluminum Oxide Templates. *Int. J. Polym. Mater. Polym. Biomater.* **2016**, *65*, 695−701.
(53) Yokoyama, H.; Kramer, E. J. Diffusion of Triblock Copolymers in a Spherical Domain Structure. *Macromolecules* **2000**, *33*, 954−959.
(54) Helfand, E.; Tagami, Y. Theory of the Interface between Immiscible Polymers. II. *J. Chem. Phys.* **1972**, *56*, 3592−3601.
(55) Mok, M. M.; Liu, X.; Bai, Z.; Lei, Y.; Lodge, T. P. Effect of Concentration on the Glass Transition and Viscoelastic Properties of Poly (Methyl Methacrylate)/ Ionic Liquid Solutions. *Macromolecules* **2011**, *44*, 1016−1025.
(56) Zeman, L.; Patterson, D. Effect of the Solvent on Polymer Incompatibility in Solution. *Macromolecules* **1972**, *5*, 513−516.
(57) Samant, S.; Strzalka, J.; Yager, K. G.; Kisslinger, K.; Grolman, D.; Basutkar, M.; Salunke, N.; Singh, G.; Berry, B.; Karim, A. Ordering Pathway of Block Copolymers under Dynamic Thermal Gradients Studied by in Situ GISAXS. *Macromolecules* **2016**, *49*, 8633−8642.
(58) Peng, J.; Gao, X.; Wei, Y.; Wang, H.; Li, B.; Han, Y. Controlling the Size of Nanostructures in Thin Films via Blending of Block Copolymers and Homopolymers. *J. Chem. Phys.* **2005**, *122*, No. 114706.
(59) Peng, J.; Xuan, Y.; Wang, H.; Li, B.; Han, Y. Solvent Vapor Induced Dewetting in Diblock Copolymer Thin Films. *Polymer* **2005**, *46*, 5767−5772.
(60) Peng, J.; Kim, D. H.; Knoll, W.; Xuan, Y.; Li, B.; Han, Y.; Knoll, W. Morphologies in Solvent-Annealed Thin Films of Symmetric Diblock Copolymer Morphologies in Solvent-Annealed Thin Films of Symmetric Diblock Copolymer. *J. Chem. Phys.* **2006**, *125*, No. 064702.
(61) Gong, J.; Ahn, H.; Kim, E.; Lee, H.; Park, S.; Lee, M.; Lee, S.; Kim, T.; Kwak, E. A.; Ryu, D. Y. Rapid Structural Reorganization in Thin Films of Block Copolymer Self-Assembly. *Soft Matter* **2012**, *8*, 3570−3575.
(62) https://pubchem.ncbi.nlm.nih.gov/compound/Heptane.
(63) https://pubchem.ncbi.nlm.nih.gov/compound/1140.

https://doi.org/10.1021/acs.macromol.1c01305
Macromolecules 2021, 54, 8512−8525